Microstructure and properties of welding joint of 8%Ni high strength steel

R. Cao[1], J. H. Chen[1], Y. Peng[2]
1.State Key Laboratory of Gansu Advanced Non-ferrous Metallic Materials and Key Laboratory of Non-ferrous Metal Alloys of the Ministry of Education, Lanzhou University of Technology，Lanzhou 730050, China
2. Central Iron and Steel Research Institute, Beijing 100081, China
* Corresponding author: zchen@lut.cn(J.H.Chen), caorui@lut.cn(R.Cao)

Abstract: This paper analyzes the mechanism of unmoral phenomena that in the HAZ of 8% Ni high strength steel, the charpy V toughness at -50℃ in the coarse grain HAZ is higher than that of fine grain HAZ. It is caused of different fracture. The former fracture is induced by void growing until impingement-resulting coalescence in the CG-specimen, and the latter fracture is caused by forming shear sheets of the secondary voids to connect the neighboring primary voids before their impingement. This paper reveals that the critical event for cleavage fracture in this high strength steel and weld metals is the propagation of a bainite packet-sized crack across the packet boundary into contiguous packets and the bainitic packet sizes control the impact toughness. The high-angle misorientation boundaries detected in a bainite packet by EBSD form fine tear ridges on fracture surfaces. However, they are not the decisive factors controlling the cleavage fracture. The effects of Ni content are essential factors for improving the toughness. The extra large cleavage facets seriously deteriorate the toughness, which are formed on the interfaces of large columnar crystals growing in welding pools with high heat input.
Keywords 980MPa 8%Ni high strength steel, weld metal, impact toughness, fracture, high-angle misorientation boundaries

1. Introduction

Due to its coarse grains and high hardenability, the CGHAZ(CG), which is overheated to a high temperature (up to 1350℃) shows a lowest ductility and toughness and limits the performance of welding structure [1]. On the contrary the FGHAZ (FG), which is heated to the normalization temperature (850-930℃) and has much finer grains, always shows the mechanical properties (including strength, ductitlity and toughness) superior than other regions within the HAZ. In the our paper, the abnormal phenomena that the Charpy V toughness in simulated CG are higher than those in the simulated FG are investigated with analyzing the different ductile fracture micromechanisms in associated microstructures formed by heating to 1320℃ and 900℃ [2]. With sustained improvement of the properties of high strength steels, the impact toughness has reached around 200J at lower temperatures of -50^{o}C for 980MPa grade steels[2]. However the toughness of the weld metals with matching strength is appreciably lower than this value. How to increase the toughness of weld metal through the modification of the microstructure has been attracting a great attention of welding metallurgists.

The microstructural parameter, which controls the toughness of weld metal may be the grain size, martensite or bainite packet size, the size of area with misorientation angle larger than 15^{o} and the brittle second phase particle size[3-8]. In this work, we use instrumented Charpy V tester, OM, SEM, TEM, EBSD and FEM calculation to identify which one in above microstructural parameters really controls the fracture and the toughness of impact Charpy V specimens. In addition, the effects of nickel addition are investigated.

2. Materials and procedures

Compositions of an 8% Ni 980MPa grade steel and various weld metals in Table 1 were used. Specimens cut in the rolling direction were heated by a heat simulating machine Thermorestor W to preset temperatures: FG (900℃), CG (1320℃), 730℃ and 600℃. The simulated heating procedures were designed as those shown in Table 2.Double heating simulations were carried out for temperatures (1320℃+1320℃, 1320℃+900℃, 1320℃+730℃, 900℃+1320℃, 900℃+900℃, and 900℃+730℃). Welding parameters of various welded joints are presented in Table 3.

The microstructures were observed by optical microscope (OP), scanning electron microscope (SEM 6700F) and transmission electron microscope (TEM JEOL2001). The grain sizes were measured by linear section method. ZEISS ULTRA 55 Field-Emission Scanning Electron Microscope was used to collect EBSD grain boundary maps and to define the orientations of microstructural features. Retained austenite films were observed by TEM and identified by selected area diffraction pattern (SADP). Tests were carried out at -50 ℃ and room temperature (RT) by universal test machine SHIMACZU AG-10 TA for tensile tests and by instrumented impact machine CIEM-30CPC for Charpy V impact tests. The average of toughness values measured in three specimens is taken as the test result. Metallographic sections are prepared by griming, polishing fracture surface of charpy specimens at -50oC to characterize the microstructural constituents and measure the grain and packet sizes just under the fracture surface. General feature and the details of fracture facets were observed on the fracture surfaces. The distances X_f from the plastic crack tip to the site of cleavage cracking initiation was measured on the fracture surfaces of specimens which were fractured o lower temperatures with short fibrous crack extension. The distances X_f is a very important parameter by which the local fracture stress σ_f, fracture strain ε_{pc} and the critical stress triaxiality T_c are calculated. The nature of crack-initiating particles was characterized.

Critical event, which controls cleavage fracture, is defined as the stage offering the most difficulty during the crack initiation and propagation. The critical event can be revealed by the cracks which retained in the fractured specimen. Metallographic sections were prepared by cutting the specimen perpendicularly to the notch root for observation of retained cracks in fractured specimens. The lengths of retained cracks are also measured by Image software.

Table 1 Compositions of experimental metals (wt%)

Sample	C	S	P	Cr	Ni	Si+Mn+Mo+Cu+Nb+V
BM	0.08	0.002	0.008	0.60	7.58	1.77
T5-21	0.07	0.005	0.005	0.71	5.74	2.71
DM4-1	0.07	0.005	0.008	0.70	3.79	2.46
M100	0.09	0.010	0.006	0.65	6.18	2.82
T100	0.07	0.004	0.008	0.63	6.36	2.7

Table 2 Parameters of simulated heat-treat procedures

E ($kJ.cm^{-1}$)	t_p(s)	T_p(℃)	t_h(s)	$t_{8/5}$(s)	$t_{5/3}$(s)
20	15	1320	2	10	24
20	11	900	1	10	24
20	8	730	1	10	24
20	7	600	1	10	24

E:Heat-input, t_p:heating time, T_p:peak temperature, t_h: holding time, $t_{8/5}$: the cooling time from 800℃ to 300℃,

Table 3 Welding method and working condition.

Welding Method	No.	Heat Input(KJ/mm)	Shielding Gas	Arc Current(A)
TIG	T5-21	2.1KJ/mm	Ar	300A
MAG	DM4-1	1.6KJ/mm	Ar+5%CO2	280A
MAG	M100	1.6KJ/mm	Ar+5%CO2	280A
TIG	T100	2.1KJ/mm	Ar	300A

3. Mechanisms of abnormal high impact toughness in simulated welding CGHAZ of an 8%Ni high strength steel

3.1 Comparison of experimental results measured in CG-specimen and FG-specimen

As seen in Fig. 1, the strengths σ_y and σ_b at -50℃ and RT measured in tensile tests of CG-specimen are lower than those measured in FG-specimen. The plasticity in terms of ψ is also higher for FG-specimen. These results consist with the microstructures shown in Fig. 2 which show the extreme larger grains in CG-specimen and middle size grains in FG. This result can be fairly inferred from the Hall-Petch rule. However as shown in Fig. 3, the values of impact toughness measured in CG-specimen at RT and -50℃ are surprisedly higher than those measured in FG-specimen. Although from Fig. 3 and Fig. 4(a), the maximum loads of Charpy V tests measured in FG-specimen are appreciably higher than those that measured in CG-specimen, yet the load drops much faster with the crack propagation. It means that in the FG-specimen the resistance to the crack propagation is lower and at same applied load the deformation then the associated strain is lower than that of CG-specimen. These phenomena make the impact toughness, particularly the crack propagation energy E_p in Fig.3 being higher for the extreme coarse grain specimen. The reason, why with lower strength and plasticity in tensile test, the CG-specimen exhibits a high resistance to crack extension in Charpy V test, is analyzed in following two paragraphs.

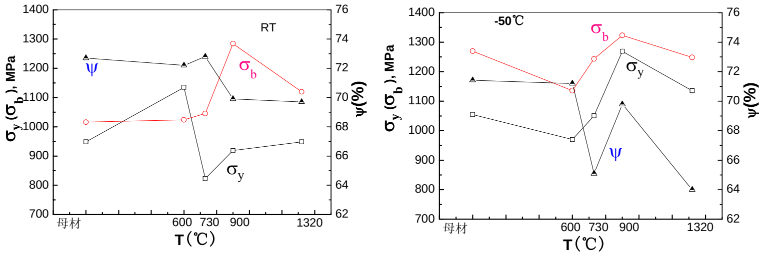

(a) (b)

Fig. 1 Results of tensile tests at RT and at -50℃

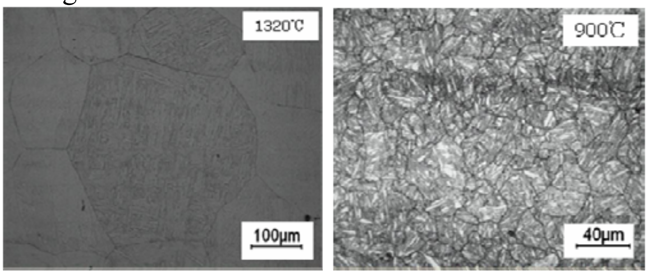

(a) Specimen ,1320℃ (b) Specimen, 900℃

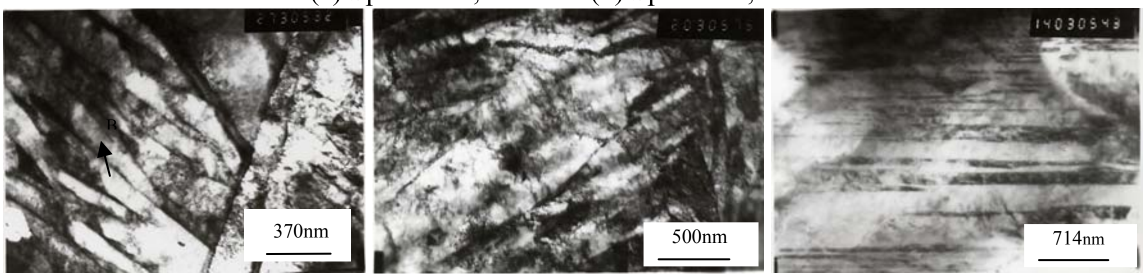

(c) Specimen ,1320℃ (d) Specimen, 900℃ (e) Specimen, 900℃

Fig. 2 Microstructures of simulated CGHAZ and FGHAZ specimen

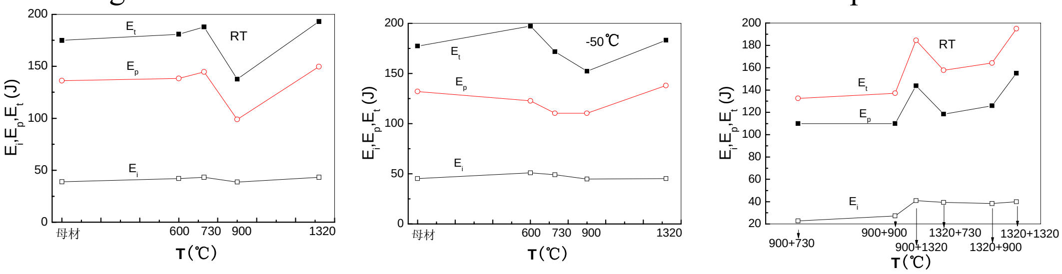

Fig. 3 The results of Charpy V tests at RT and at -50℃

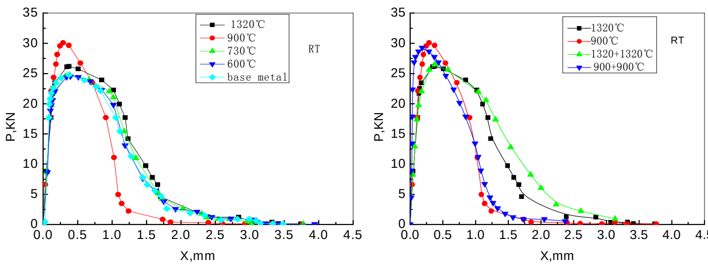

Fig. 4 Load-displacement plots measured by the instrumented impact machine(a) specimens by single heating (b) Comparison of effects of single and double heating

3.2 Different micro-mechanisms of rupture for CG-specimen and FG-specimen.

Fig. 5(a) shows the fracture surfaces of Charpy V specimen of CG. It is apparent that the ductile rupture is caused by the primary voids, which nucleate, grow until impingement-resulting coalescence and final rupture. In this case the rupture obeys the criterion of critical void growth. According to the void growth model of Rice and Tracey [7]:

$$\frac{dR}{R} = A \cdot e^{(\frac{3\sigma_m}{2\sigma_{eq}})} d\varepsilon_{eq} \qquad (1)$$

the critical radius R_c can be expressed [7] as

$$Ln(\frac{R_c}{R_0}) = 0.283\varepsilon_f^{(\frac{3\sigma_m}{2\sigma_{eq}})} \qquad (2)$$

The fracture strain ε_f increases with increasing the critical radius R_c at same stress triaxiality σ_m/σ_{eq}. As shown in Fig. 5(a) the critical radius R_c of the primary voids grow to as large as 100μm, close to the size of the lath bainite packets. Thus the corresponding fracture strain ε_f should reach a higher level and provides a higher resistance to crack propagation. However for FG-specimen, as shown in Fig. 5(b), the final rupture is caused by the shear sheets formed by numerous secondary voids, which connect the primary voids long before their impingement. Thus in FG-specimen the final rupture happens at less ε_f, once it can produce the secondary voids to connect the primary voids before they reach to impinge. Thus the primary voids in FG grow to much smaller size (Fig.5(b)) than those growing in specimen-CG(Fig. 5(a)). The total plastic strain, then the energy spent in fracture is less for the FG-specimen than for the CG-specimen. From Fig. 5, it is found that for both CG-specimen and FG-specimen, the primary voids are nucleated by inclusions, which leave black holes at the centers of the primary voids. But the original phase, which nucleates numerous small secondary voids in FG specimens cannot be identified in the fracture surfaces. Fig. 6 show fracture surfaces in same magnification, one for FG specimen (a) and the other for CG specimen (b). In Fig. 6(a) two primary voids (1 and 2) of 20-40 μm are connected by small secondary voids and numerous small secondary voids distribute on the fracture surface. In Fig. 6(b), two large primary voids (100μm in sizes) coalesce directly. Apparent plastic striations are present on void surfaces however on whole vision field no secondary void is produced.

From above analyses, the key point is the production of numerous secondary voids in the FG-specimen at a lower plastic strain, while in the CG-specimen only a few of second voids are produced even at the fracture strain. By comparing the fracture surfaces (Fig. 5(b) and the microstructures (Fig. 2(a), it is found that the sizes of primary voids correspond to the bainite packets (20-30μm) and the secondary voids correspond to the bainitic laths. Fig.2 (d) and (e) shows the transmission electron micrographs of FG-specimens. Fig.2 (d) shows the lath bainitic without carbide precipitation. The martensite laths with the width in the range of 0.2-0.4μm is consider to be much more brittle than the bainite laths. It is then inferred that the laths of the martensite are broken and nucleate the second voids at a lower level of plastic strain, before the primary voids grow to impingement and coalescence.

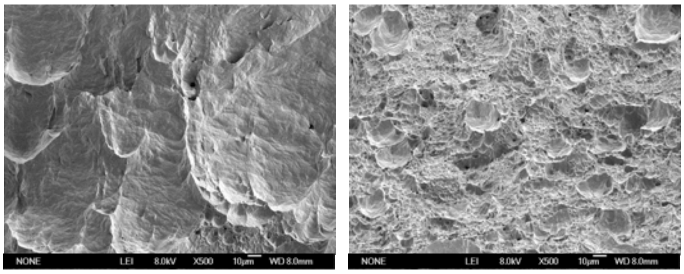

(a) Specimen ,1320℃ 198J, RT (b) Specimen, 900℃, 142J, RT

Fig. 5 Fracture surfaces of Charpy V tested specimen (a) heated to 1320(b) heated to 900 ℃

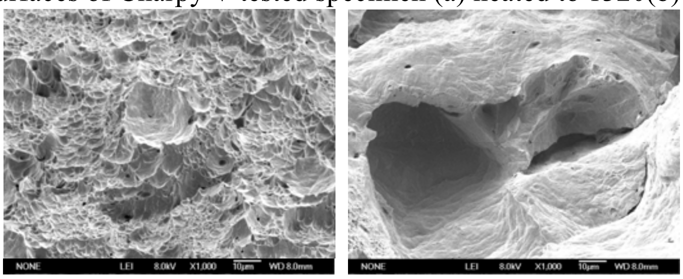

(a) (b)

Fig. 6 Fracture surfaces showing the details of rupture (a) by connection of numerous secondary voids in FG and (b) by coalescence of large primary voids in CG

By comparing the fracture surface (Fig. 5 (a) and the microstructure (Fig. 2(a)) of CG specimens, the primary voids correspond to the large bainitic packets. The tiny carbide plates (only 0.01*0.04μm in size) precipitated inside the bainite are considered being not able to nucleate small voids. It can be concluded that although the grain sizes of CG specimens are extreme large, yet due to the high temperature (1320℃) heating, the carbon content is unified in the original austenite grain. After fast cooling the lath bainite microstructure keeps uniform in carbon content without local accumulation. The sizes of the carbide precipitation plates inside the bainitic lath are very small (only 0.01*0.04μm in size). The carbide plates with such tiny size can only be broken and nucleate the voids at a high level of plastic strain, however this high plastic strain cannot be reached before the coalescence of the primary voids in a notched Charpy V specimen with high stress triaxiality. And just this high stress triaxiality increases the rate of primary void growth.

3.3 Effects of stress triaxiality on the nucleation and growth of the voids

Fig. 1 show that both the strengths at -50℃ and RT measured in tensile tests of specimen CG are lower than those measured in specimen FG, while the Charpy V toughness is higher. The reason is analyzed as follows

Fig.7 shows fracture surfaces of CG-specimen (a) and (b) and that of FG-specimen (c) fractured by tensile tests at RT. Comparing Fig.5(a) and Fig. 7(a) for CG-specimen, it can be found that: in the impact test, the fracture is dominated by primary voids, which grow until impingement-resulting coalescence and final rupture, while in the tensile test the final rupture is caused by the secondary voids which connect the neighboring primary voids before their impingement. In FG-specimen, the fracture surfaces for both impact test (Fig. 5(b)) and tensile test (Fig. 7(b)) show rupture being caused by the shear sheets formed by numerous secondary voids which connect the neighboring primary voids long before their impingement. Therefore, the phenomena, that the CG-specimen shows the abnormal superior impact toughness, but the inferior tensile properties, can be attributed to the change of fracture mechanisms from the primary void-coalescence in the notch impact test to the secondary void-connection in the tensile test. In Charpy V tests, the energy, which is spent on the fracture by void growing until impingement-resulting coalescence in the CG-specimen is higher than that spent in the FG-specimen where the fracture is caused by forming shear sheets of the secondary voids to connect the neighboring primary voids before their impingement. However, in tensile tests, both CG-specimen and FG-specimen are fractured with the similar mechanism of connection of the primary voids by the secondary voids. The tensile properties of the CG-specimen are inferior due to its intrinsic inferiority such as large grain size.

Then the question is why for the CG-specimen, the fracture mechanism is changed from primary void coalescence in the Charpy V test to the secondary void connection in the tensile test. It is attributed to the difference of the stress triaxialities between these two types of tests. In the Charpy V impact test, because the stress triaxiality at the the notch is high, up to 1.6 by FEM calculation, while in the tensile test it varies from 0.33 to approximate 1.0 from a smooth specimen to a necking one at area reduction of 65 -70%. According to formula (2) $Ln(R_c/R_o) = 0.283\varepsilon_f(3\sigma_m/2\ \sigma_{eq})$, for the Charpy V specimen with a high stress triaxiality σ_m/σ_{eq}, the critical void radius R_c is reached at a lower fracture strain ε_f, which cannot cause the breaking of the tiny carbide plates precipitated inside the bainite laths or cause the breaking of the bainite laths in the CG-specimen. Therefore no (or only a few) secondary voids are produced in the fracture process (Fig. 6(b)). However, in the FG-specimen, the brittle martensite laths are broken at a less strain level and form numerous second voids, which connect the insufficiently growing primary voids and make an early fracture and lower toughness. In the tensile tests, the stress triaxiality is low and the plastic strain, which can reach is high. Even, in the CG-specimen, the secondary voids can be nucleated by the breaking bainitic laths (Fig.2(d)) before the impingement of the primary voids. The final fracture is caused also by the connection of insufficiently growing primary voids by the second voids (As shown in Fig. 7(a)).

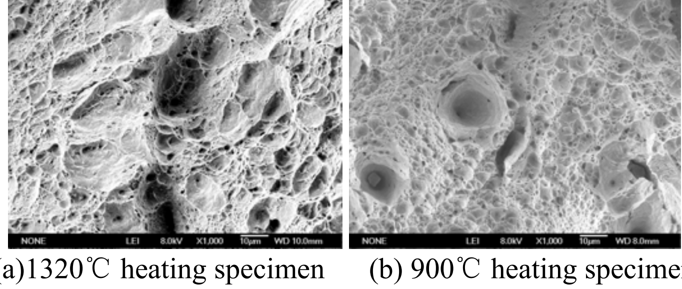

(a)1320℃ heating specimen (b) 900℃ heating specimen

Fig. 7 Fracture surfaces of specimens fractured at RT by tensile tests (a) 1320℃, (b) 900℃

4. Relationships between the microstructures and properties

The values of impact toughness measured by the instrumented Charpy V tester at temperature range from -196°C to 20°C are plotted in Fig. 8. Corresponded welding parameters and compositions are presented in Table 3.The effects on charpy toughness will be analyzed from followed aspects.

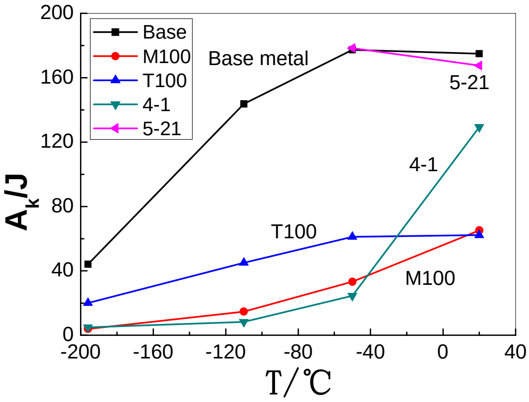

Fig 8. Charpy V values measured at various temperatures

From Fig. 8 it is found that the base metal and weld metal can be divided to two group according to the toughness measured at -50°C. The first group includes the base metal, T5-21 weld metals which present much higher impact toughness at -50°C. The second group includes DM4-1, M100 and T100, which show appreciable lower impact toughness. In following, the experimental results are focused to find the factors determining the difference of the cryogenic low temperature impact toughness between these two groups in the high strength steel and weld metals.

Fig. 9 displays the general microstructures of base metal and all weld metals. As seen in Fig. 9, the microstructure of base metal is the typical tempered lath bainite. The weld metals of T5-21 exhibit a little coarser lath bainite, and those of DM4-1 show somewhat appearance of globular bainite with some acicular ferrite. The distinct characteristics of weld metals of M100 and T100 are the black trips which are considered to be traces of segregation on the boundaries of columnar crystals growing in the weld pools. However, the remarked difference in impact toughness of metals cannot be simply attributed to the difference of these microstructures. Followed several aspects will be analyzed.

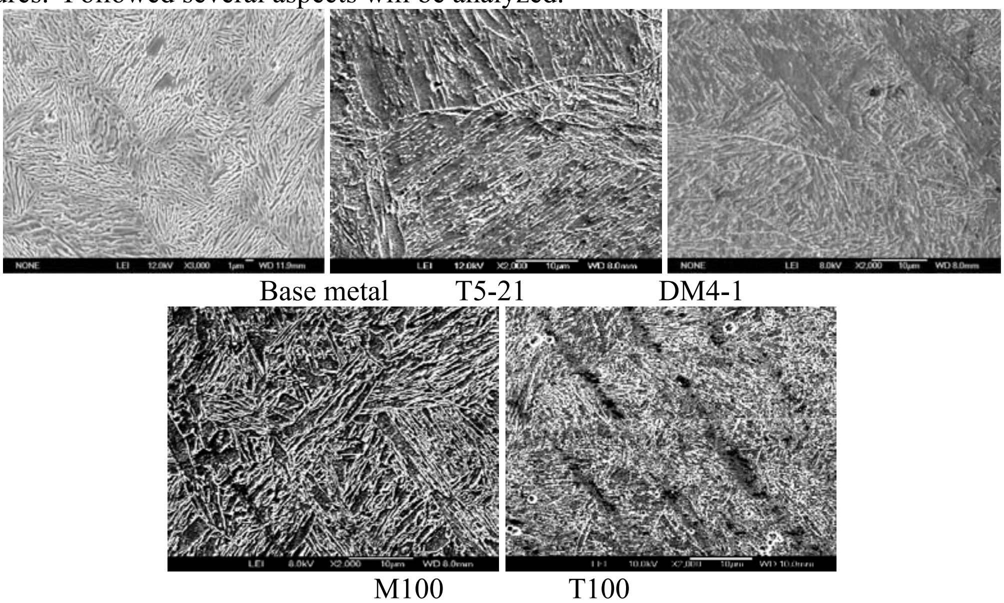

Fig 9. The microstructures of base metal and all weld metals

4.1 critical event

The critical event is the most difficult step in the crack nucleation and propagation process, which controls the cleavage fracture. The main methodology for identifying the critical event was suggested by the present author [9]. Fig. 10 shows the cracks retained in base metal and weld metal in Charpy V specimens fractured at -196°C. The lengths of retained cracks and the lengths of packets measured by random events are plotted in right side figures. From Fig.10 in the metallographic sections of the fractured specimens, the cracks stopped at the packet boundaries, thus retained cracks were constrained in the bainitic packets in the Base metal, DM4-1, M100 and T100. And there is a consistent relationship between the lengths of the retained cracks and the sizes of the bainitic packets. Based on these experimental observations, the critical events for cleavage fracture in base metal and the weld metals are identified as the propagation of a packet-sized crack across the packet boundary into contiguous packets.

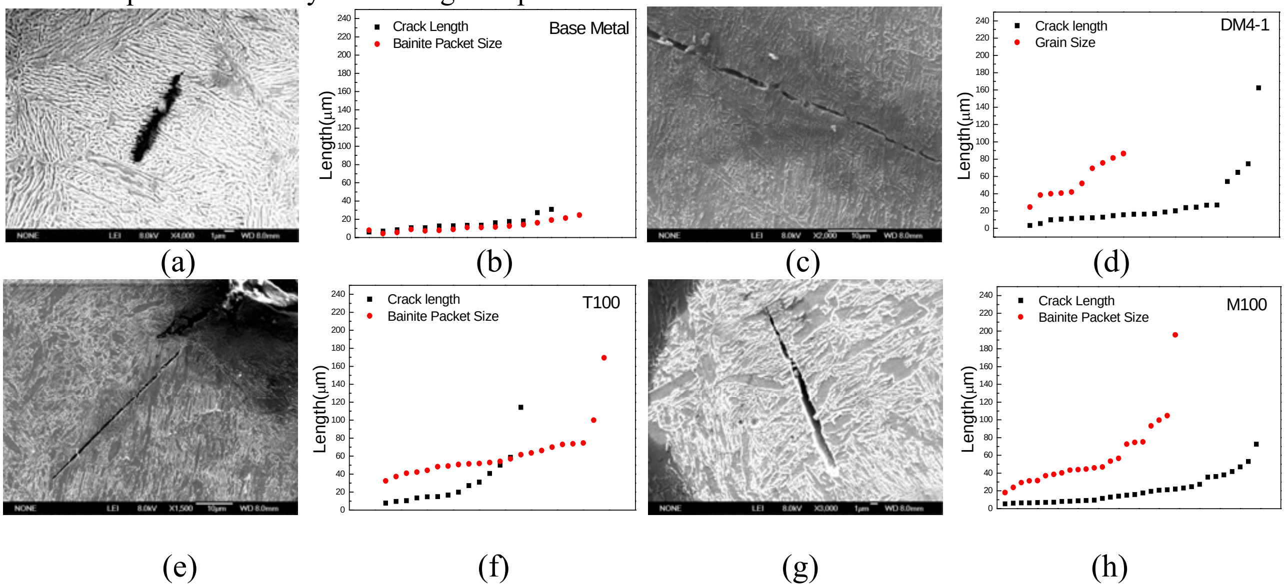

Fig 10. The cracks retained in base metal and weld metal in Charpy V specimens fractured at -196°C and the lengths of retained cracks and bainitic packets randomly measured by random event in (a) (b) base metal (c) (d) DM4-1(e) (f) T100 (g) (h) M100

4.2 Critical micro-parameters

Through the FEM calculation, the values of σ_f, ε_{pc} and T_c for base metal and weld metal DM4-1, T100 and M100 are obtained and listed in Table 3. The corresponding impact toughness measured at -196°C are listed in the Table 4. As seen in the Table 3 the local fracture stress σ_f measured in base metal are much higher than those measured in the weld metal DM4-1, T100 and M100. This is corresponded with the values of impact toughness listed in the Table 3. Table 4 lists the effective surface energy γ_p calculated from the σ_f and the area of the cleavage facet observed in front of the crack initiation site by equation. The areas of the cleavage facets observed in front of the crack initiation sites listed in Table 4 are in the order consistent with the order of packets' sizes in Fig. 12 and the calculated values of γ_p are reasonable.

Table 3 Results of calculation of σ_f, ε_{pc}, T_c

	T (℃)	P_y (KN)	P_m (KN)	σ_{yd} (MPa)	E_{-196}(J)	SCL (μm)	X_f (μm)	σ_f (MPa)	ε_{pc}	Tc
MC	-196	26.476	31.521	1236.93	44.2	600	251	2705	0.0242	1.33
DM4-1	-196	26.47	10	1236.80	5.9	0	289	1591	0	0.95
T100	-196	24.03	16.975	1158.19	20.0	275	469	1988	0.00137	1.045
M100	-196	24.79	6.57	1122.73	3.9	10	110	1581	0.00148	0.75

T ;test temperature, P_y: impact yield load, P_m: impact maximum load, σ_{yd}: impact yield strength, SZW: width of stretch zone, X_f: distance from the crack initiation site to the plastic crack tip, σ_f: local fracture stress, ε_{pc}: fracture strain, T_C: critical stress triaxiality

$$\sigma_f = \sqrt{\pi E \gamma p/(1-\upsilon^2)a} \quad \text{(for a penny-shaped crack)}$$

Table 4 Effective surface energy calculated from σ_f and the cleavage facet area

	σ_f	E	ν	a	C_0	γ_p
MC	2705	200000	0.3	22	0.43	233.26
DM4-1	1591	200000	0.3	39.7	0.73	145.62
T100	1988	200000	0.3	40	0.33	229.07
M100	1581	200000	0.3	37.7	0.45	136.55

σ_f: Local fracture stress, E: Young's modulus, ν: Poisson's ratio, a: cleavage facet area, C_o: size of second phase particle, γ_p: effective surface energy

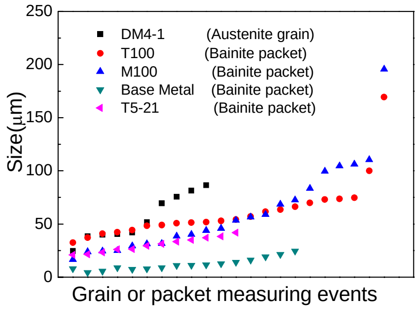

Fig 12. The grain and packet sizes measured in successive events

4.3 Effects of high degree misorientation boundaries

As stated in the introduction, Ref. [7] revealed that bainitic packet size measured by EBSD is identified as the microstructural unit controlling crack propagation in a cleavage fracture. Fig. 13 displays the higher degree misorientation boundaries depicted by EBSD for base metal and weld metals. From Fig.13, the fraction of area contained by the higher degree misorientation boundaries for the base metal is the smallest among all microstructures. Fig. 14 exhibits the histograms of the degrees of grain or packet boundaries.

In this study, as seen in Fig. 13, the sizes of the areas contained by the high misorientation degree boundaries are appreciably smaller than the sizes of the bainitic packets, however, in Fig. 10, the retained cracks are stopped by the packet boundaries, rather than by the high misorientation degree boundaries in a packet. Thus, the cleavage fracture is controlled by the bainitic packet rather than by the area contained by the high misorientation degree boundaries. In addition as shown in Fig. 13 and Fig. 14, there are not appreciable differences of the densities of high degree misorientation boundaries revealed by EBSD for T5-21and DM4-1 metals. To be surprised, the density of high degree misorientation boundaries in base metal is appreciably lower than that of weld metals. Therefore the superior impact toughness of base metal and T5-21 at -50°C cannot be attributed to the difference of the density of high degree misorientation boundaries.

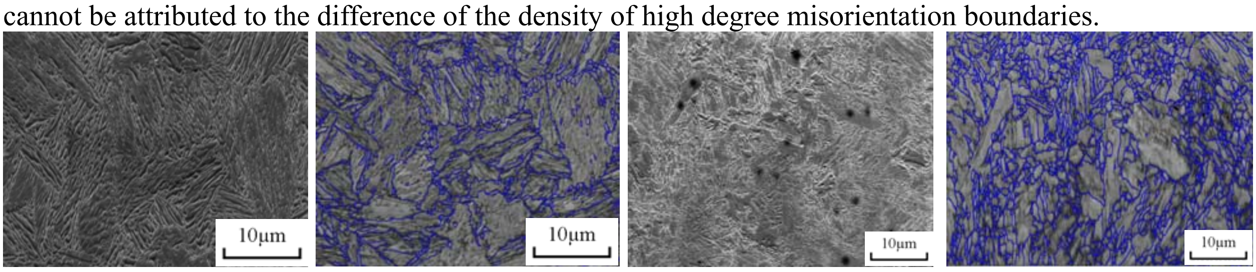

(a)Base metal (b)T5-21

(c)DM4-1 (d)M100

Fig 13. The higher degree misorientation boundaries depicted by EBSD for (a) base metal and weld metals (b) T5-21 (c) DM4-1 (d) M100 weld metals

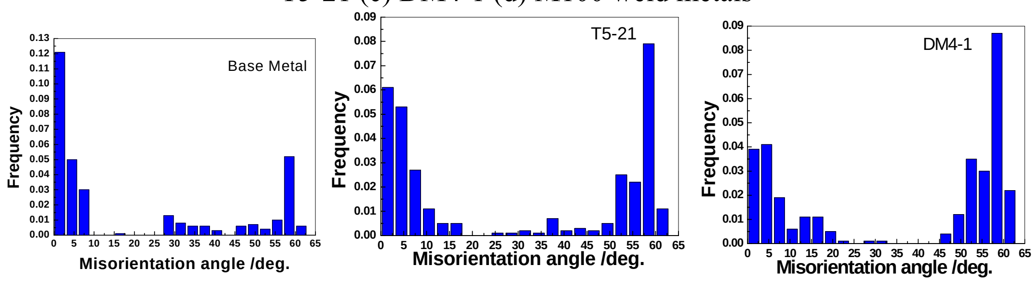

(a) (b) (c)

Fig 14. Histograms of the degrees of grain or packet boundaries of (a)base metal (b) T5-21 (c) DM4-1

As shown in Fig. 13 there is not appreciate differences of the densities of high degree misorientation boundaries revealed by EBSD for T5-21 and DM4-1 metals. To be surprised, the density of high degree misorientation boundaries in base metal is appreciably lower than those of weld metals.

In followed Fig. 15, by comparing the high misorientation degree boundaries and the fine tear ridges in the cleavage facets, it seems that the latter is produced by the former. Thus, in this study, the resistance to the cleavage cracking is mainly provided by the packet boundary, and the high misorientation degree boundaries offers some resistance and produce the fine tear ridges in the cleavage facets.

4.4 Decisive microstructural constituents

Based on the above discussions, it is concluded that the decisive microstructural feature which determines the impact toughness in the notched bar is the bainite packet rather than the region contained by the high misorientation degree boundaries. The bainite boundary provides the main resistance and makes the propagation of a packet-sized crack across the boundary the critical event for the cleavage fracture. The packet size specifies the critical cleavage facet and the local fracture stress σ_f. The reason why the values of impact toughness measured at -50^{o}C for base metal, and T5-21 are generally higher than those measured for DM4-1, T100 and M100 is attributed to that the size of the bainitic packet of the former group is finer than that of the latter group. Fig. 16 shows a typical comparison between the packet sizes of the DM4-1 weld metal and the T5-21 weld metal. It is apparently that the sizes of packets in T5-21 are appreciably smaller than that in DM4-1 weld metal. The general comparison of the grain or the packet sizes is summarized in Fig. 12. As the lengths of the critical events corresponding to the sizes of packets of the first group of the base metal and T5-21 are smaller than that of the second group of DM4-1, T100 and M100. This is the reason why the impact toughness of the metals of the first group is superior to that of the metals of the second group.

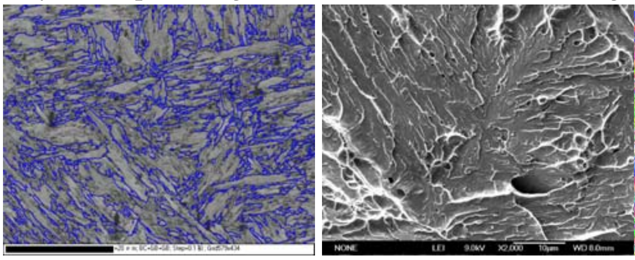

Fig 15. Comparing the high misorientation degree boundaries and the fine tear ridges on the fracture surface

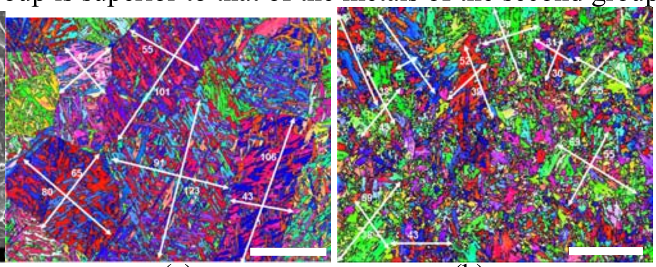

(a) (b)

Fig 16. Sizes of packets in (a)DM4-1 (b) T5-21

4.5 Effects of nickel addition

As indicated in the introduction, Ref.[8] revealed that regardless of packet size and yield strength, the addition of nickel gave rise to a decrease in Charpy V impact transition temperature of about 20^{o}C per percent nickel. He attributed this effect to increasing the cleavage fracture resistance [8]. In this work at first the metals were divided to two groups: the first group including MC and T5-21 which presents superior impact toughness and the second group including DM4-1 which presents inferior toughness. From the composition point of view, the only appreciable distinction in alloy content is the difference in Ni contents: around 6-7% Ni for the first group and lower than 4%Ni for the second group. The effects of Ni addition were focused. Table 5 compares the relative parameters between the two groups. As seen in Table 5, the grain sizes of weld metals with higher Ni contents are finer. Besides the fine grain/packet sizes in the metals of the higher Ni content group, the fine bainitic laths and the higher fractions of the M-A constituent were observed. Because in steels with higher Ni content the flaks of the M-A constituent were found to be rich of austenite and have high plasticity[10], both fine bainitic laths and Ni-rich M-A flakes causes denser higher misorientation boundaries and higher resistance by the appearance of fine tear ridges on the fracture surface. The effect of Ni addition is considered to be decisive in the difference of impact toughness between these two groups. The mechanism of the improvement needs to be investigated in future.

Table 5 Parameters relevant to Ni content and toughness (drawn from Table 5)

No.	$E_{-50}{}^oC$ (J)	Nickel (%)	Average grain size(μm)	Width of Bainite lath(nm)	Average width of Bainite lath (nm)	Area fraction of M-A(%)
MC	177	7.58	20	20-80	34	58
T5-21	163	5.74	30	65-186	113	39
DM4-1	24.5	3.79	60	180-850	428	26

4.6 Effect of welding process

Table 6 lists the values of Charpy V impact toughness and relevant parameters measured at -50^{o}C for weld metals of T100 and T5-21.

Table 6 Parameters relevant to Ni content and toughness

No.	$E_{-50}{}^{o}C$ (J)	Nickel (%)	Average grain size(μm)	Width of Bainite lath(nm)	Average value (nm)	Area fraction of M-A(%)
T5-21	163	5.74	30	65-186	113	39
T100	61.2	6.36	60	59-578	151	26

As listed in Table 6, while the Ni content of 6.36% in T100 weld metal is comparable with that of 5.74% in T5-21. However, the impact toughness of 61.2J of the former is much less than that of 163J in the latter. In addition, the grain sizes and the width of bainitic laths of T100 are larger than that of T5-21, the area fraction of M-A flakes is less for T100 than for T5-21. The reason which causes the inferior toughness and the factors deteriorating the toughness is attributed to the welding process. Fig. 17 displays the fracture surface (a) and the macrostructure (b and c) of the weld metal T100. From Fig. 17 it is evident that the coarse directional columnar grains exhibited in Fig. 17 (c) produce the coarse embossing fracture strips shown in Fig.17 (a) which cause the inferior toughness of weld metal T100. Table 7 lists the metallographic parameters measured in T100 and T5-21 weld metal which shows that the width of the weld of T100 is appreciably larger than that of T5-21. It is considered to be welded by horizontal weaving of the welding torch. This procedure produces high heat input at same welding current and causes larger columnar grains and segregation of impurities on the boundaries of the crystalline cells as shown in Fig. 17(b) and (c). Therefore, regardless of the higher nickel content the large columnar grains with impurity segregating boundaries make the impact toughness of the T100 weld metal inferior. The similar phenomenon was observed in the case of M100.

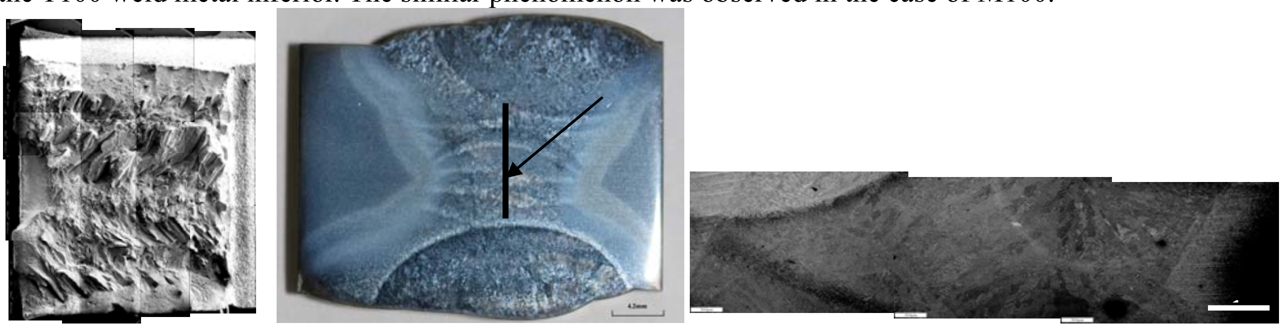

(a) (b) (c)

Fig 17. The fracture surface (a) and the macrostructure (b and c) of the weld metal T100

Table 11 Metallographic parameters measured in T100 and T5-21 weld metal

Weld metal	Weld Width (mm)	Weld depth (mm)	Columnar grain width (mm)	Sizes of fine grain (mm)
T5-21	15.9	7.4	0.29	0.11
T100	20	7.6	0.41	0.45
M100	14.3	8.5	0.47	0.16

Acknowledgements

This work was financially supported by National Nature Science Foundation of China (No. 51035004 and 51265028).

References

[1] D. Chae, C. J. YoungD. M. Goto and D. A. Koss, Metall. Mater. Trans. A, 32A(2001)2229-2237
[2] R. Cao, W.Feng, Y. Peng, W. S. Du, Z. L. Tian, J. H. Chen, Mater.Sci.Eng A. 528(2010) 631-642.
[3] J. R. Low, Deformation and fracture in solids, Springer-Verlag, Berlin, (1956) 163-176.
[4] Kamada, N. Koshizuka, T.Funakoshi, Transaction ISIJ, 16(1976)407-416.
[5] G. T. Hahn, Metall. Trans. A. 15(1984)947–959.
[6] A.Echeverria, J. M. Rodriques-Ibabe, Mater.Sci.Eng A. 346(2003)149-158.
[7] L.Rancel, M. Gomez, S. F. Medina, I. Gutierrez, Mater.Sci.Eng A. 530(2011) 21-27.
[8] R. Cao, Y. J. Yan, W. S. Du, Z. L. Tian, Y. Peng, J. H. Chen, 2011, Mater.Sc.Techno, 27(2011)145-155.
[9] J. H. Chen, G. Z. Wang, C. Yan, H. Ma, and L. Zhu, Inter. J. Fract. 83(1997)105-120.